molecules

MDPI

*Article*

# On the Jahn–Teller Effect in Silver Complexes of Dimethyl Amino Phenyl Substituted Phthalocyanine †

**Martin Breza**

Department of Physical Chemistry, Slovak Technical University, Radlinskeho 9, SK-81237 Bratislava, Slovakia; martin.breza@stuba.sk

† Dedicated to Professor Andrej Staško in honor of his 85th birthday.

**Abstract:** The structures of Ag complexes with dimethyl amino phenyl substituted phthalocyanine $^{m}$[dmaphPcAg]$^{q}$ of various charges q and in the two lowest spin states m were optimized using the B3LYP method within the $D_{4h}$ symmetry group and its subgroups. The most stable reaction intermediate in the supposed photoinitiation reaction is $^{3}$[dmaphPcAg]$^{-}$. Group-theoretical analysis of the optimized structures and of their electron states reveals two symmetry-descent mechanisms. The stable structures of maximal symmetry of complexes $^{1}$[dmaphPcAg]$^{+}$, $^{3}$[dmaphPcAg]$^{+}$, $^{2}$[dmaphPcAg]$^{0}$, and $^{4}$[dmaphPcAg]$^{2-}$ correspond to the $D_4$ group as a consequence of the pseudo-Jahn–Teller effect within unstable $D_{4h}$ structure. Complexes $^{4}$[dmaphPcAg]$^{0}$, $^{1}$[dmaphPcAg]$^{-}$, $^{3}$[dmaphPcAg]$^{-}$, and $^{2}$[dmaphPcAg]$^{2-}$ with double degenerate electron ground states in $D_{4h}$ symmetry structures undergo a symmetry descent to stable structures corresponding to maximal $D_2$ symmetry, not because of a simple Jahn–Teller effect but due to a hidden pseudo-Jahn–Teller effect (strong vibronic interaction between excited electron states). The reduction of the neutral photoinitiator causes symmetry descent to its anionic intermediate because of vibronic interactions that must significantly affect the polymerization reactions.

**Keywords:** DFT; TD-DFT; symmetry descent; electron states; vibronic interactions



**Citation:** Breza, M. On the Jahn–Teller Effect in Silver Complexes of Dimethyl Amino Phenyl Substituted Phthalocyanine. *Molecules* **2023**, *28*, 7019. https://doi.org/10.3390/molecules28207019

Academic Editor: Adriana Dinescu

Received: 9 September 2023
Revised: 3 October 2023
Accepted: 9 October 2023
Published: 10 October 2023



## 1. Introduction

New photosensitive systems with improved efficiency for initiating free-radical and/or cationic polymerizations under light activation are developed using sophisticated chemical treatments. Very recently, Breloy et al. [1] synthesized dimethyl amino substituted phthalocyanine dmaphPcH$_2$ and its Ag(II) complex $^{2}$[dmaphPcAg]$^{0}$ (Figure 1). Photoexcitation of [dmaphPcAg]$^{0}$ in the presence and absence of an iodonium salt produced acidic and radical species that initiated cationic and free-radical polymerizations, respectively. The photoinitiator properties were investigated via spectroscopic and quantum-chemical methods. The polymerization kinetics in laminate and under air was studied. In the first step, irradiation (385 and 405 nm) caused a reduction of Ag(II) to Ag(I), and nitrogen-centered radicals were formed. Subsequently, Ag nanoparticles and carbon-centered radicals developed. Intermediates [dmaphPc]$^{-}$, Ag$^{0}$ nanoparticles, and [dmaphPcAg]$^{q}$ complexes, q = $-1 \rightarrow +1$, are supposed within the proposed reaction mechanism. DFT calculations indicate a $D_4 \rightarrow D_2$ symmetry descent in [dmaphPcAg]$^{q}$ complexes which could be ascribed to the Jahn–Teller (JT) effect. The aim of our recent study is to shed more light on this problem and to verify the above explanation using a group-theoretical analysis of the DFT-optimized structures of [dmaphPcAg]$^{q}$ complexes within the highest possible $D_{4h}$ symmetry group and its subgroups.

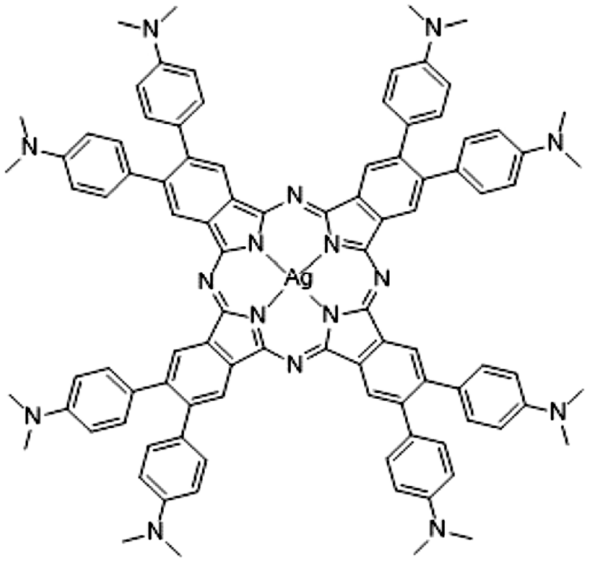


**Figure 1.** Structure of $^{2}$[dmaphPcAg]$^{0}$ [1].

## 2. Theoretical Background

According to the Jahn–Teller theorem [2], any nonlinear configuration of atomic nuclei in a degenerate electron state is unstable. Hence, there is at least one such configuration of lower symmetry where the above degeneracy is removed. In other words, the multidimensional representation in the high-symmetric (HS) structure is split into nondegenerate representations in the low-symmetric (LS) structure.

The JT active coordinate $Q_{JT}$ describes the abovementioned symmetry descent. If the potential energy surface $E = f(Q_i)$ of N atoms is a function of $3N - 6$ independent nuclear coordinates $Q_i$, for the JT 'unstable' HS structure, the following relation for any $Q_{JT}$ is valid:

$$\left(\frac{\partial E}{\partial Q_{JT}}\right)_{HS} \neq 0 \quad (1)$$

The HS $\rightarrow$ LS geometry change described by $Q_{JT}$ is connected with an energy decrease which is denoted as the JT stabilization energy $E_{JT:}$

$$E_{JT} = E_{HS} - E_{LS} \quad (2)$$

An analogous symmetry descent and energy decrease for pseudodegenerate electron states is known as the pseudo-Jahn–Teller (PJT) effect. It can be observed for a sufficiently strong vibronic interaction and relatively small energy difference $\Delta_{ij}$ between the interacting electron states $\Psi_i$ and $\Psi_j$ [3].

In some cases, the existence of LS structures cannot be explained by the JT effect of the degenerate ground electron state nor by the PJT interactions of the non-degenerate ground electron state with low-lying excited states in the HS structure (e.g., because of their different spin multiplicity). (P)JT effects in these cases are "hidden" in the excited states, which can undergo vibronic interactions as well. The vibronic interaction within the degenerate excited state or between two (or more) excited states of suitable symmetries can be so strong that the lower energy surface penetrates the potential surface of the ground electron state corresponding the HS structure and becomes the lowest state in the LS structure (i.e., its ground electron state). These consequences of the strong JT and PJT vibronic interactions within excited electron states are known as the hidden JT (HJT) and hidden PJT (HPJT) effects, respectively [4].

(P)JT potential surfaces can be described using an analytical function based on perturbation theory. In the simplest case of single distortion coordinate $Q$ and double electron

degeneracy or two interacting electron states of different symmetries, we obtain their potential energy surface $E(Q)$ in the form

$$E(Q) = \frac{1}{2}KQ^2 \pm [\frac{\Delta_{ij}^2}{4} + F^2Q^2]^{1/2} \quad (3)$$

where $\Delta_{ij} = 0$ for double electron degeneracy (JT effect) or $\Delta_{ij} > 0$ is the energy difference between both interacting electron states (PJT effect) in the undistorted geometry, $K$ is the primary force constant (without vibronic coupling), and $F$ is the vibronic coupling constant [3]. However, the search for their extremal points corresponding to the 'stable' or 'unstable' (P)JT structures is too complicated for large molecular systems. In such cases, a group-theoretical treatment must be used.

The epikernel principle method [5,6] is based on the $Q_{JT}$ symmetry in the HS structure. A nonzero value of the integral

$$< \Psi_i \left| \frac{\partial \hat{H}}{\partial Q_{JT}} \right| \Psi_j > \neq 0 \quad (4)$$

for the interacting electron states $\Psi_i$ and $\Psi_j$ and the full-symmetric Hamilton operator $\hat{H}$ demands that the direct product

$$\Gamma_i{}^* \otimes \Lambda_{JT} \otimes \Gamma_j \quad (5)$$

where $\Gamma_i$, $\Lambda_{JT}$, and $\Gamma_j$ are representations of $\Psi_i$, $Q_{JT}$, and $\Psi_j$, respectively (the asterisk denotes a complex conjugate value), must contain a full-symmetric representation. Alternatively:

$$\Lambda_{JT} \in \Gamma_i{}^* \otimes \Gamma_j \quad (6)$$

In the case of the JT effect and the degenerate states $\Psi_i = \Psi_j$, i.e., $\Gamma_i = \Gamma_j$, we obtain the even stronger condition

$$\Lambda_{JT} \in [\Gamma_i \otimes \Gamma_i]^+ \quad (7)$$

where $[\ldots]^+$ denotes the symmetric direct product.

The epikernel principle states that the extrema of a JT energy surface correspond to the kernel K(G, $\Lambda_{JT}$) or epikernel E(G, $\Lambda_{JT}$) subgroups of the HS parent group G. Kernels contain the symmetry operations of G that leave the $\Lambda_{JT}$ representation invariant. The symmetry operations of epikernels leave invariant only some components of the degenerate $\Lambda_{JT}$ representation.

The epikernel principle was originally formulated for the systems in degenerate electron states only [5,6], but it has been successfully extended (except Equation (7)) to pseudodegenerate electron states as well [7]. Its drawback is in the restriction to JT active coordinates that have been derived within perturbation theory for the linear Taylor expansion of the perturbation only. This method might offer incomplete results in some cases (e.g., in systems with $C_5$ rotations) [7].

The method of step-by-step symmetry descent [8,9] is based on consecutive splitting of a degenerate electron state within a JT symmetry descent. The vibronic interaction causes instability of the HS structure, and thus, in the sense of the JT theorem [2], some symmetry elements are removed. The probability of the symmetry elements removal decreases with the number of these elements. It implies that the symmetry decrease to the immediate subgroups with the lowest number of the removed symmetry elements are more probable than to other subgroups. The multidimensional representation corresponding to the degenerate electron state can be split within symmetry descent to an immediate subgroup of the parent HS group G (see Table S1 in Supplementary Materials). If the structure corresponding to this subgroup is in a nondegenerate electron state, it is JT stable and the symmetry descent stops. If the structure corresponding to an immediate subgroup of G is in a degenerate electron state described by a multidimensional representation (a JT unstable structure), the symmetry descent continues to its immediate subgroups and

the whole procedure is repeated. As every group can have several immediate subgroups, various symmetry descent paths are possible and the JT stable structures can correspond to various LS symmetry groups. The only condition is its nondegenerate electron state (i.e., one-dimensional representation), obtained through splitting the degenerate electron state (i.e., multidimensional representation) of the HS structure of the parent group G.

## 3. Results

The highest possible structures of [dmaphPcAg]$^{q}$ complexes are of the $D_{4h}$ symmetry group with side phenyl groups perpendicular to the central phthalocyanine plane (Figure 2). Because of the great number of possible mutual orientations of dimethyl amino phenyl groups in less symmetric structures, we restricted our study to the stable structures of the maximal symmetry group only. Another restriction is implied by the inability of standard DFT methods to optimize the atomic configurations in degenerate electron states [10]. The results of the geometry optimizations of the $^{m}$[dmaphPcAg]$^{q}$ complexes with total charges q = +1 $\rightarrow$ −2 in the two lowest spin states m are presented in Table 1. It is interesting that the [dmaphPcAg]$^{q}$ complexes in the triplet spin state are more stable than these ones with the same charge in the singlet spin state. $^{3}$[dmaphPcAg]$^{-}$ of $D_2$ symmetry is the most stable complex under study. It must be mentioned that the use of an unrestricted 'broken symmetry' treatment [11] results in zero spin populations and does not reduce the energy of the systems studied. Therefore, only the restricted Kohn–Sham formalism has been used in subsequent TD-DFT calculations of our complexes in singlet ground states.

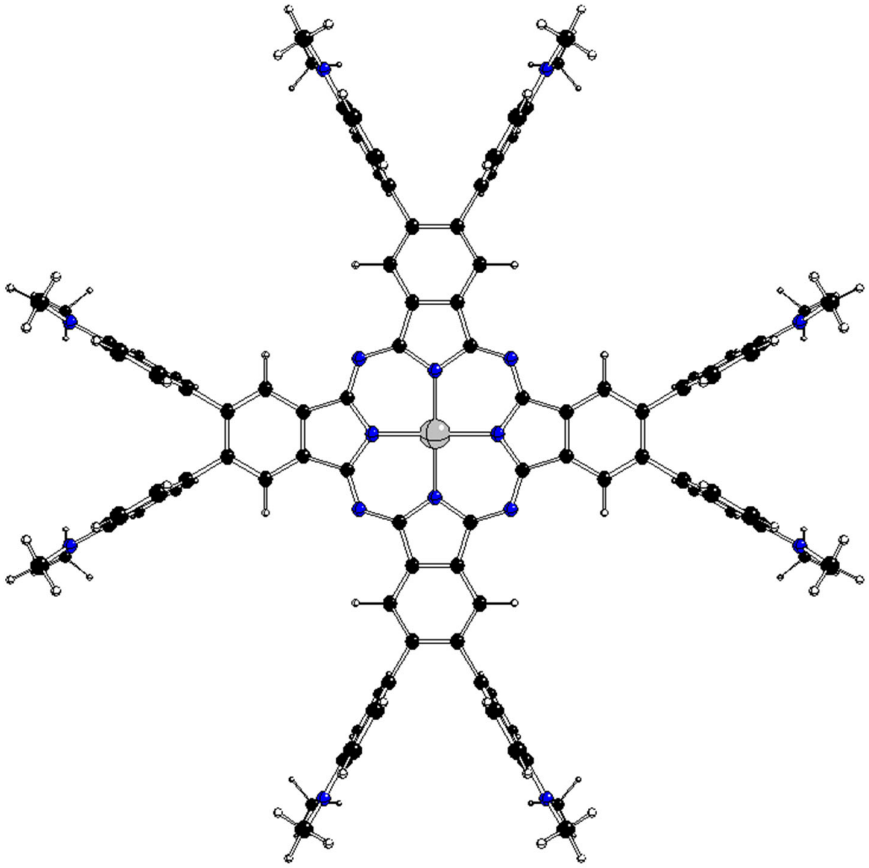

**Figure 2.** Optimized $D_{4h}$ structure of $^{2}$[dmaphPcAg]$^{0}$ (C—black, N—blue, H—white, Ag—grey).

**Table 1.** Charge q, spin multiplicity m, symmetry group G, representation of the ground electron state $\Gamma_0$, DFT energy $E_{DFT}$, JT stabilization energy $E_{JT}$, representations $\Lambda_{im}$ and wavenumbers $\nu_{im}$ of imaginary vibrations, kernel K($D_{4h}$, $\Lambda_{im}$) and epikernel K($D_{4h}$, $\Lambda_{im}$) subgroups of $D_{4h}$, and representations of relevant PJT excited states $\Gamma_{exc}$ of $^{m}$[dmaphPc]$^{q}$ complexes under study (the preserved symmetry elements in the kernel and epikernel subgroups are in parentheses). The most stable structure is shown in bold.

| q | m | G | $\Gamma_0$ | $E_{DFT}$ [Hartree] | $E_{JT}$ [eV] | $\Lambda_{im}$ | $\nu_{im}$ [cm$^{-1}$] | K($D_{4h}$, $\Lambda_{im}$) | E($D_{4h}$, $\Lambda_{im}$) | $\Gamma_{exc}$ |
|---|---|---|---|---|---|---|---|---|---|---|
| +1 | 1 | $D_{4h}$ | $^1A_{1g}$ | −4734.55067 | - | $b_{1u}$ | −48 | $D_{2d}(C_2')$ | | $B_{1u}$ |
| | | | | | | $2e_g$ | −47, −31 | $C_1$ | $C_{2h}(C_2')$, $C_{2h}(C_2'')$ | $E_g$ |
| | | | | | | $a_{1u}$ | −46 | $D_4$ | | $A_{1u}$ |
| | | | | | | $a_{2u}$ | −31 | $C_{4v}$ | | $A_{2u}$ |
| | | | | | | $b_{2u}$ | −31 | $D_{2d}(C_2'')$ | | $B_{2u}$ |
| +1 | 1 | $D_4$ | $^1A_1$ | −4734.58352 | 0.894 | - | - | | | |
| +1 | 3 | $D_{4h}$ | $^3B_{1u}$ | −4734.54698 | - | $b_{1u}$ | −18 | $D_{2d}(C_2')$ | | $A_{1g}$ |
| | | | | | | $e_g$ | −18 | $C_1$ | $C_{2h}(C_2')$, $C_{2h}(C_2'')$ | $E_u$ |
| | | | | | | $a_{1u}$ | −18 | $D_4$ | | $B_{1g}$ |
| +1 | 3 | $D_4$ | $^3B_1$ | −4734.58550 | 1.048 | - | - | | | |
| 0 | 2 | $D_{4h}$ | $^2B_{1g}$ | −4734.74708 | - | $b_{1u}$ | −42 | $D_{2d}(C_2')$ | | $A_{1u}$ |
| | | | | | | $e_g$ | −42 | $C_1$ | $C_{2h}(C_2')$, $C_{2h}(C_2'')$ | $E_g$ |
| | | | | | | $a_{1u}$ | −41 | $D_4$ | | $B_{1u}$ |
| | | | | | | $a_{2u}$ | −23 | $C_{4v}$ | | $B_{2u}$ |
| | | | | | | $3b_{2u}$ | −23(3×) | $D_{2d}(C_2'')$ | | $A_{2u}$ |
| 0 | 2 | $D_4$ | $^2B_1$ | −4734.77283 | 0.701 | - | - | | | |
| 0 | 4 | $D_2$ | $^4B_2$ | −4734.73113 | unknown | - | - | | | |
| −1 | 1 | $D_2$ | $^1A$ | −4734.79846 | unknown | - | - | | | |
| **−1** | **3** | **$D_2$** | **$^3B_2$** | **−4734.83355** | unknown | - | - | | | |
| −2 | 2 | $D_2$ | $^2B_1$ | −4734.80520 | unknown | - | - | | | |
| −2 | 4 | $D_{4h}$ | $^4B_{1u}$ | −4734.77355 | - | $b_{1u}$ | −47 | $D_{2d}(C_2')$ | | $A_{1g}$ |
| | | | | | | $2e_g$ | −46, −27 | $C_1$ | $C_{2h}(C_2')$, $C_{2h}(C_2'')$ | $E_u$ |
| | | | | | | $a_{1u}$ | −45 | $D_4$ | | $B_{1g}$ |
| | | | | | | $a_{2u}$ | −27 | $C_{4v}$ | | $B_{2g}$ |
| | | | | | | $b_{2u}$ | −27 | $D_{2d}(C_2'')$ | | $A_{2g}$ |
| −2 | 4 | $D_4$ | $^4B_1$ | −4734.80581 | 0.878 | - | - | | | |

Further inspection of Table 1 shows that the studied complexes can be divided into two categories:

(i) Category I contains complexes $^1$[dmaphPcAg]$^+$, $^3$[dmaphPcAg]$^+$, $^2$[dmaphPcAg]$^0$, and $^4$[dmaphPcAg]$^{2-}$ with optimized structures of $D_{4h}$ (unstable) and $D_4$ (stable) symmetry groups.

(ii) Category II contains complexes $^4$[dmaphPcAg]$^0$, $^1$[dmaphPcAg]$^-$, $^3$[dmaphPcAg]$^-$, and $^2$[dmaphPcAg]$^{2-}$, where only their stable optimized structures of the $D_2$ symmetry group were found, while the $D_{4h}$ optimized structures were absent. This can be explained by the electron configurations of the $D_{4h}$ complexes in Table 2. We may conclude that the category II complexes should contain partially occupied $e_g$ molecular orbitals, which implies $E_g$ or $E_u$ ground electron states. Hence, they are not accessible through standard DFT methods.

**Table 2.** Charge q, spin multiplicity m, electron configuration, and ground electron state representation $\Gamma_0$ of studied $^{m}$[dmaphPc]$^{q}$ complexes of $D_{4h}$ symmetry group.

| q | m | Electron Configuration | $\Gamma_0$ |
|---|---|---|---|
| +1 | 1 | $\ldots(b_{2g})^2(e_u)^4(a_{2g})^2(b_{1g})^0(e_g)^0(b_{1u})^0\ldots$ | $^1A_{1g}$ |
| +1 | 3 | $\alpha$: $\ldots(b_{1g})^1(a_{2g})^1(e_u)^2(b_{2g})^1(e_g)^0(b_{1u})^0\ldots$<br>$\beta$: $\ldots(e_u)^2(b_{2g})^1(a_{1u})^0(e_g)^0(b_{1g})^0(b_{1u})^0\ldots$ | $^3B_{1u}$ |
| 0 | 2 | $\alpha$:$\ldots(e_u)^2(b_{2g})^1(b_{1g})^1(a_{1u})^1(e_g)^0(b_{1u})^0\ldots$<br>$\beta$:$\ldots(e_u)^2(b_{2g})^1(a_{1u})^1(e_g)^0(b_{1g})^0(b_{1u})^0\ldots$ | $^2B_{1g}$ |
| 0 | 4 | unknown | $^4E_g$ or $^4E_u$ |
| −1 | 1 | unknown | $^1E_g$ or $^1E_u$ |
| −1 | 3 | unknown | $^3E_g$ or $^3E_u$ |
| −2 | 2 | unknown | $^2E_g$ or $^2E_u$ |
| −2 | 4 | $\alpha$:$\ldots(e_g)^2(b_{2g})^1(a_{1u})^1(b_{1g})^1(e_g)^2(b_{2u})^0\ldots$<br>$\beta$:$\ldots(e_g)^2(a_{2u})^1(a_{1u})^1(e_g)^0(a_{2u})^0(b_{2u})^0\ldots$ | $^4B_{1u}$ |

### *3.1. Category I Complexes*

The optimized $D_{4h}$ structures of these complexes are unstable due to several imaginary vibrations of $\Lambda_{im}$ representations (Table 1) that coincide with the JT active coordinates. The JT stabilization energies $E_{JT}$ correspond to $D_{4h} \rightarrow D_4$ symmetry decrease. Stable $D_4$ structures with equally rotated phenyl rings (Figure 3) and without any imaginary vibration correspond to the K($D_{4h}$, $\Lambda_{im}$) kernel subgroups for the coordinate of the $a_{1u}$ representation. As indicated by its wavenumber $\nu_{im}$, the energies of the corresponding vibrations are comparable with the highest energy ones in all category I complexes. The optimized structures of $D_{2d}$ and $C_{4v}$ symmetries are not stable (not presented), and hence only the $D_4$ ones fulfill the condition of the stable structure of the highest symmetry group.

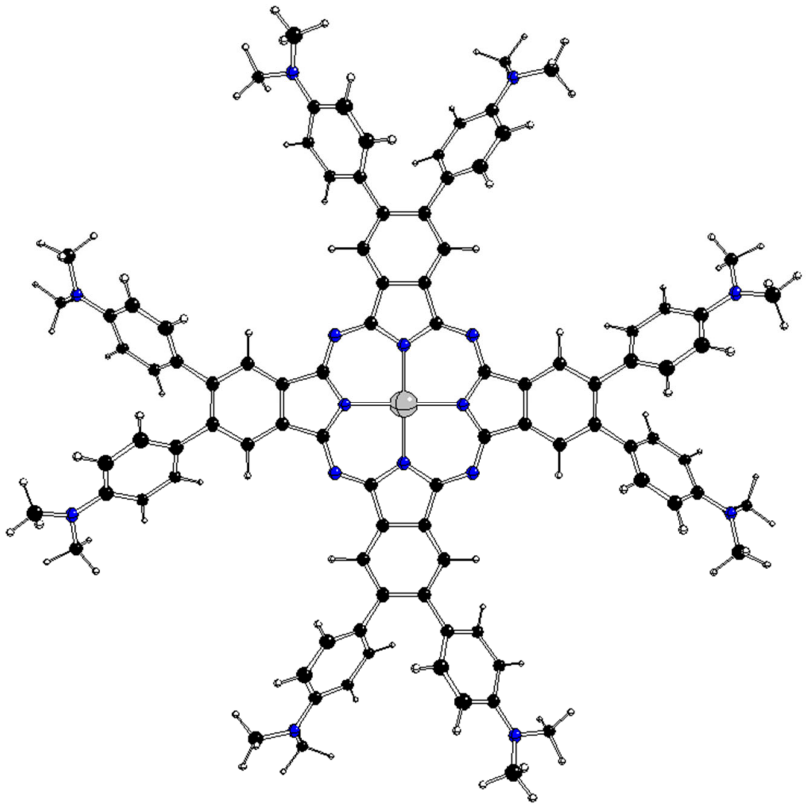

**Figure 3.** Optimized $D_4$ structure of $^2$[dmaphPcAg]$^0$ (see Figure 2 for atom notation).

For known ground state $\Gamma_0$ and JT coordinate $\Lambda_{im}$ representations, the Equations (4) and (5) can be used to determine the excited-state representations $\Gamma_{exc}$ (see Table 1) interacting with the ground electron state in $D_{4h}$ structures of our complexes. The comparison of the TD-DFT calculated electron states in the corresponding $D_{4h}$ and $D_4$ structures (Table 3) shows that the energy difference $E_{exc}$ between the PJT interacting states increases after symmetry descent as a consequence of their vibronic interaction. This confirms the correct assignment of the corresponding states in both groups because the standard treatment based on similarity of their oscillator strengths $f$ is hardly usable in our cases. The ground states in the $D_{4h}$ structures also correspond to those in their $D_4$ subgroups.

**Table 3.** Charge q, spin multiplicity m, symmetry group G, ground electron state representation $\Gamma_0$, representations $\Gamma_{exc}$, excitation energies $E_{exc}$, and oscillator strengths $f$ of the low excited electron states of the studied $^{m}$[dmaphPc]$^{q}$ complexes in $D_{4h}$ and $D_4$ symmetry groups. The excited states that interact with the ground states are in bold.

| q | m | G | $\Gamma_0$ | $\Gamma_{exc}$ | $E_{exc}$ [eV] | $f$ | G | $\Gamma_0$ | $\Gamma_{exc}$ | $E_{exc}$ [eV] | $f$ |
|---|---|---|---|---|---|---|---|---|---|---|---|
| +1 | 1 | $D_{4h}$ | $^1A_{1g}$ | $1^1A_{2g}$ | 0.156 | 0.000 | $D_4$ | $^1A_1$ | $1^1B_1$ | 0.167 | 0.000 |
| | | | | $1^1E_u$ | 0.158 | 0.002 | | | $1^1B_2$ | 0.255 | 0.000 |
| | | | | $1^1B_{2g}$ | 0.159 | 0.000 | | | $1^1E$ | 0.259 | 0.000 |
| | | | | $1^1B_{1g}$ | 0.349 | 0.000 | | | $1^1A_2$ | 0.267 | 0.000 |
| | | | | $2^1E_u$ | 0.353 | 0.081 | | | $2^1E$ | 0.631 | 0.014 |
| | | | | $1^1B_{1u}$ | 0.377 | 0.000 | | | $1^1A_1$ | 0.642 | 0.000 |
| | | | | $1^1A_{1g}$ | 0.487 | 0.000 | | | $2^1B_1$ | 0.858 | 0.000 |
| | | | | $1^1E_g$ | 1.010 | 0.000 | | | $3^1E$ | 1.187 | 0.050 |
| | | | | **$1^1A_{1u}$** | **1.010** | **0.000** | | | **$2^1A_1$** | **1.192** | **0.001** |
| | | | | $1^1B_{1u}$ | 1.010 | 0.000 | | | $2^1A_2$ | 1.200 | 0.000 |
| +1 | 3 | $D_{4h}$ | $^3B_{1u}$ | $1^3B_{2g}$ | 0.011 | 0.000 | $D_4$ | $^3B_1$ | $1^3E$ | 0.188 | 0.007 |
| | | | | $1^3A_{2g}$ | 0.015 | 0.001 | | | $1^3B_2$ | 0.190 | 0.000 |
| | | | | $1^3E_u$ | 0.016 | 0.001 | | | $1^3A_2$ | 0.195 | 0.000 |
| | | | | **$1^3A_{1g}$** | **0.235** | **0.000** | | | **$1^3A_1$** | **0.600** | **0.000** |
| | | | | $2^3E_u$ | 0.235 | 0.014 | | | $2^3E$ | 0.617 | 0.298 |
| | | | | $1^3B_{2u}$ | 0.239 | 0.000 | | | $1^3B_1$ | 0.779 | 0.000 |
| | | | | $2^3E_u$ | 1.255 | 0.000 | | | $3^3E$ | 1.244 | 0.001 |
| | | | | $3^3E_u$ | 1.327 | 0.003 | | | $4^3E$ | 1.391 | 0.033 |
| | | | | $1^3E_g$ | 1.493 | 0.008 | | | $2^3B_1$ | 1.400 | 0.000 |
| 0 | 2 | $D_{4h}$ | $^2B_{1g}$ | $1^2E_u$ | 1.195 | 0.000 | $D_4$ | $^2B_1$ | $1^2E$ | 1.157 | 0.000 |
| | | | | $1^2E_g$ | 1.306 | 0.000 | | | $2^2E$ | 1.305 | 0.000 |
| | | | | **$1^2B_{1u}$** | **2.014** | **0.000** | | | $3^2E$ | 1.901 | 0.624 |
| | | | | $2^2E_u$ | 2.050 | 0.710 | | | $1^2B_2$ | 1.942 | 0.000 |
| | | | | $2^2E_g$ | 2.140 | 0.000 | | | $1^2A_2$ | 1.944 | 0.000 |
| | | | | $1^2B_{2u}$ | 2.140 | 0.000 | | | $4^2E$ | 1.956 | 0.004 |
| | | | | $1^2A_{2u}$ | 2.140 | 0.000 | | | $2^2A_2$ | 1.969 | 0.000 |
| | | | | $3^2E_g$ | 2.163 | 0.000 | | | $1^2A_1$ | 2.055 | 0.000 |
| | | | | $2^2B_{2u}$ | 2.164 | 0.000 | | | $3^2A_2$ | 2.056 | 0.000 |
| | | | | $2^2A_{2u}$ | 2.164 | 0.000 | | | **$1^2B_1$** | **2.059** | **0.001** |
| −2 | 4 | $D_{4h}$ | $^4B_{1u}$ | $1^4E_g$ | 0.957 | 0.000 | $D_4$ | $^4B_1$ | $1^4E$ | 0.888 | 0.191 |
| | | | | $1^4A_{2u}$ | 0.976 | 0.000 | | | $1^4B_1$ | 1.356 | 0.000 |
| | | | | $1^4B_{2u}$ | 0.978 | 0.000 | | | $2^4E$ | 1.360 | 0.010 |
| | | | | $2^4E_g$ | 1.025 | 0.000 | | | $1^4A_1$ | 1.360 | 0.000 |
| | | | | $1^4A_{1u}$ | 1.042 | 0.000 | | | $3^4E$ | 1.396 | 0.010 |
| | | | | $1^4B_{1u}$ | 1.048 | 0.000 | | | $1^4A_2$ | 1.415 | 0.000 |
| | | | | $3^4E_g$ | 1.118 | 0.110 | | | $1^4B_2$ | 1.417 | 0.000 |
| | | | | $1^4A_{1g}$ | 1.495 | 0.000 | | | $4^4E$ | 1.436 | 0.012 |
| | | | | **$1^4B_{1g}$** | **1.495** | **0.000** | | | $2^4B_2$ | 1.472 | 0.001 |
| | | | | $1^4E_u$ | 1.496 | 0.000 | | | $2^4A_2$ | 1.481 | 0.000 |
| | | | | $2^4A_{1u}$ | 1.501 | 0.000 | | | **$3^4B_1$** | **1.523** | **0.000** |

We can see (Table 3) that the PJT active excited states in the $D_{4h}$ structures are relatively high. This indicates that their excitation energies are less important for possible vibronic interactions than the energies of JT active coordinates.

### *3.2. Category II Complexes*

As mentioned above, the ground state of the $D_{4h}$ structures of these complexes is double degenerate ($E_g$ or $E_u$ representations), and only the stable $D_2$ structures (Figure 4) were obtained through geometry optimizations. Possible representations of the corresponding JT active coordinates can be obtained via the symmetric direct products for the HS group:

$$[E_g \otimes E_g]^+ = [E_u \otimes E_u]^+ = A_{1g} \oplus B_{1g} \oplus B_{2g} \quad (8)$$

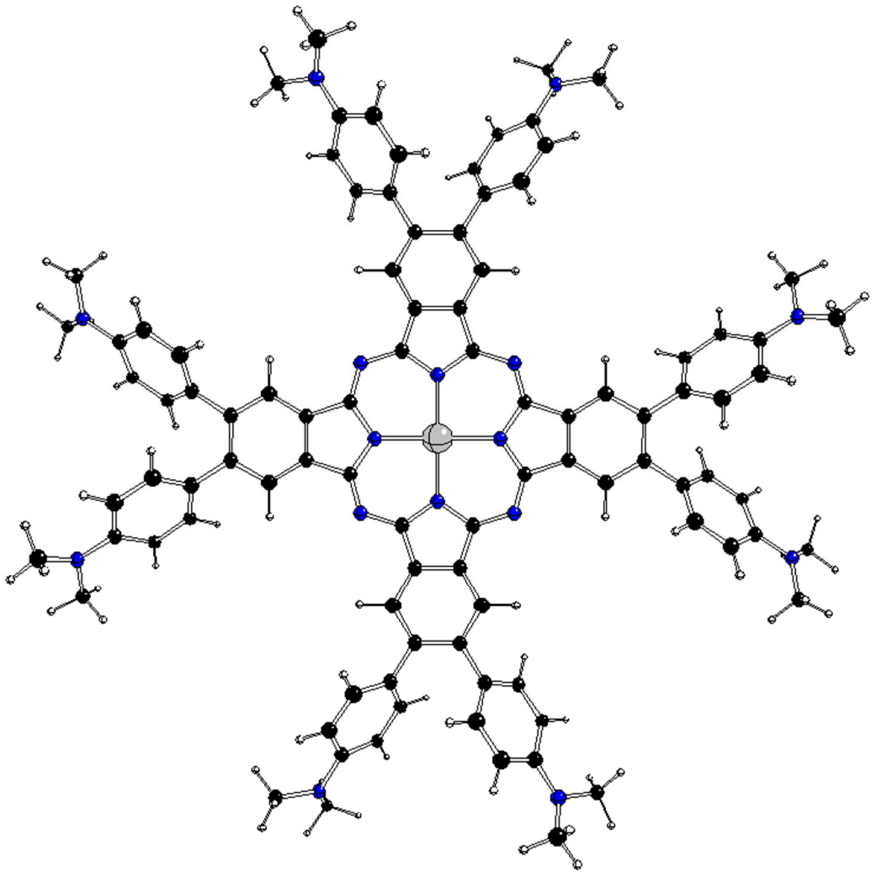

**Figure 4.** Optimized $D_2$ structure of $^1[dmaphPcAg]^-$ (see Figure 2 for atom notation).

The full-symmetric $a_{1g}$ coordinate does not change the symmetry of the structure (i.e., cannot be JT active) and the kernels

$$K(D_{4h}, b_{1g}) = D_{2h}(C_2') \quad (9)$$

$$K(D_{4h}, b_{2g}) = D_{2h}(C_2'') \quad (10)$$

do not explain the existence of the optimized $D_2$ structure. Therefore, the method of the epikernel principle [5,6] cannot explain the $D_{4h} \rightarrow D_2$ symmetry descent.

The method of step-by-step symmetry descent [8,9] for the structures of the $D_{4h}$ symmetry group in double degenerate electron states is based on the scheme in Figure 5. Except $D_{2h}$, all immediate subgroups of the $D_{4h}$ group (i.e., $D_4$, $D_{2d}$, $C_{4v}$, and $C_{4h}$) are JT unstable because of preserved electron degeneracy. After the removal of the $C_4$ axis from the

$D_4$ group, we obtain its immediate subgroup $D_2$, which is JT stable because the degeneracy is removed here. Alternatively, the $D_2$ group can be obtained via symmetry descent through the JT unstable $D_{2d}$ group with preserved electron degeneracy. The structures of the $C_4$ and $S_4$ symmetry groups preserve electron degeneracy and therefore cannot be stable. We have not found any stable structure of $D_{2h}$, $C_{2v}$, or $C_{2h}$ symmetry groups through geometry optimization. Therefore, the stable $D_2$ structures meet the condition of maximal groups for category II complexes.

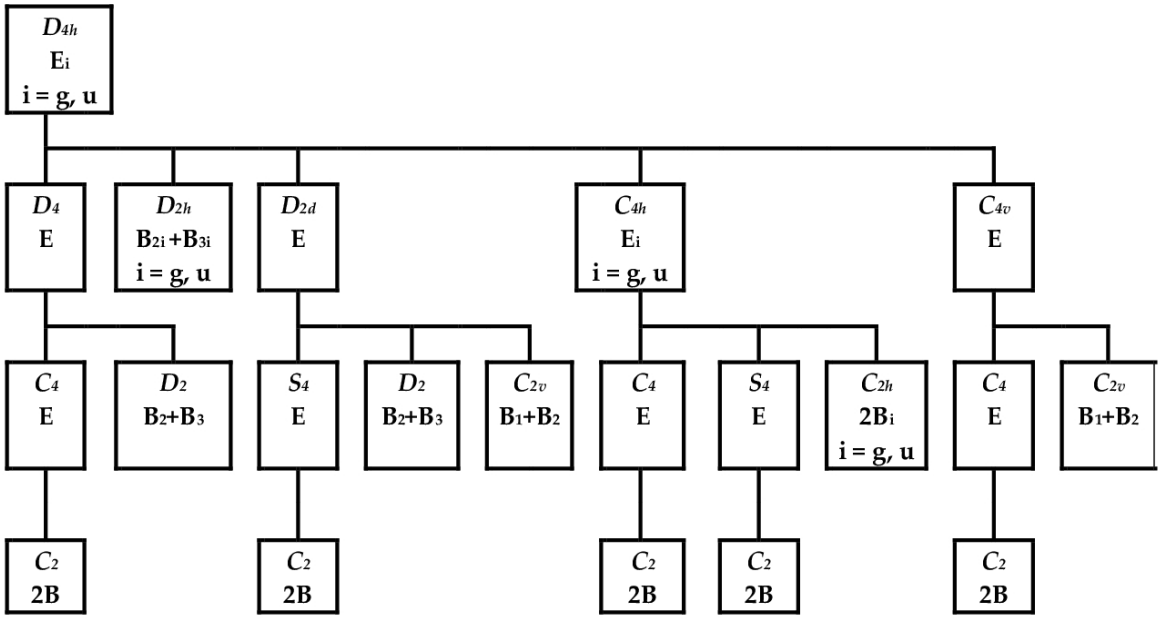


**Figure 5.** Possible symmetry descent paths of $D_{4h}$ structures in double degenerate electron states [9]. The top and bottom lines of individual rectangles denote symmetry groups and the corresponding irreducible representations, respectively.

During the symmetry descent from $D_{4h}$ to $D_2$, the double degenerate representation is split into the nondegenerate $B_2$ and $B_3$ ones:

$$E_g \text{ or } E_u\ (D_{4h}) \rightarrow E\ (D_4 \text{ or } D_{2d}) \rightarrow B_2 \oplus B_3\ (D_2) \tag{11}$$

None of these representations corresponds to the calculated ground electron state of the stable $D_2$ structures (Table 4). This discrepancy can be explained using the above-mentioned HPJT effect, and the ground state of the $D_2$ structure corresponds to the lower PJT interacting excited state in its supergroup. In our case, the situation is complicated by the fact that $D_2$ is not an immediate subgroup of the $D_{4h}$ group. Therefore, there are three possible two-step symmetry descent paths:

$$D_{4h} \xrightarrow{a_{1u}} D_4 \xrightarrow{b_1 \text{ or } b_2} D_2 \tag{12}$$

$$D_{4h} \xrightarrow{b_{1g} \text{ or } b_{2g}} D_{2h} \xrightarrow{a_u} D_2 \tag{13}$$

$$D_{4h} \xrightarrow{b_{1u} \text{ or } b_{2u}} D_{2d} \xrightarrow{b_1} D_2 \tag{14}$$

**Table 4.** Charge q, spin multiplicity m, representations of the ground electron state $\Gamma_0$ and of the excited states $\Gamma_{exc}$, excitation energies $E_{exc}$, and oscillator strengths $f$ of low excited electron states of stable $^{m}$[dmaphPc]$^{q}$ complexes under study in the $D_2$ symmetry group. The irreducible representations obtained through splitting the two-dimensional representations of the degenerate ground state in $D_{4h}$ structures are in bold.

| q | m | $\Gamma_0$ | $\Gamma_{exc}$ | $E_{exc}$ [eV] | $f$ | q | m | $\Gamma_0$ | $\Gamma_{exc}$ | $E_{exc}$ [eV] | $f$ |
|---|---|---|---|---|---|---|---|---|---|---|---|
| 0 | 4 | $^4B_2$ | $1^4B_1$ | 0.349 | 0.000 | −1 | 1 | $^1A$ | $\mathbf{1^1B_2}$ | **0.523** | **0.000** |
| | | | $\mathbf{1^4B_3}$ | **0.814** | **0.012** | | | | $1^1B_1$ | 0.539 | 0.000 |
| | | | $2^4B_1$ | 0.829 | 0.000 | | | | $\mathbf{1^1B_3}$ | **0.815** | **0.000** |
| | | | $\mathbf{1^4B_2}$ | **0.927** | **0.006** | | | | $2^1B_2$ | 1.337 | 0.023 |
| | | | $3^4B_1$ | 0.948 | 0.000 | | | | $2^1B_3$ | 1.478 | 0.028 |
| | | | $2^4B_3$ | 1.253 | 0.000 | | | | $3^1B_2$ | 1.551 | 0.005 |
| | | | $2^4B_2$ | 1.254 | 0.213 | | | | $4^1B_2$ | 1.793 | 0.809 |
| | | | $1^4A$ | 1.291 | 0.000 | | | | $3^1B_3$ | 1.965 | 0.018 |
| | | | $3^4B_3$ | 1.356 | 0.164 | | | | $1^1A$ | 2.056 | 0.000 |
| | | | $2^4A$ | 1.423 | 0.000 | | | | $4^1B_3$ | 2.097 | 0.011 |
| −1 | 3 | $^3B_2$ | $1^3B_1$ | 0.272 | 0.000 | −2 | 2 | $^2B_1$ | $1^2B_1$ | 0.048 | 0.000 |
| | | | $1^3B_3$ | 1.256 | 0.000 | | | | $2^2B_1$ | 0.377 | 0.000 |
| | | | $\mathbf{1^3B_2}$ | **1.350** | **0.021** | | | | $1^2B_2$ | 0.900 | 0.007 |
| | | | $\mathbf{2^3B_3}$ | **1.356** | **0.014** | | | | $\mathbf{2^2B_2}$ | **1.095** | **0.283** |
| | | | $2^3B_2$ | 1.796 | 0.792 | | | | $\mathbf{1^2B_3}$ | **1.112** | **0.306** |
| | | | $3^3B_3$ | 1.835 | 0.007 | | | | $3^2B_2$ | 1.168 | 0.000 |
| | | | $4^3B_3$ | 1.987 | 0.012 | | | | $1^2A$ | 1.343 | 0.000 |
| | | | $1^3A$ | 1.993 | 0.000 | | | | $4^2B_2$ | 1.348 | 0.002 |
| | | | $2^3B_1$ | 2.000 | 0.000 | | | | $2^2A$ | 1.362 | 0.000 |
| | | | $2^3A$ | 2.092 | 0.000 | | | | $2^2B_3$ | 1.367 | 0.002 |

Based on group–subgroup relations, we can assign the electron state representations of the $D_2$ symmetry group to the corresponding $D_4$, $D_{2h}$, or $D_{2d}$ ones despite the several alternatives. The same holds for the $D_{4h}$ to $D_4$, $D_{2h}$, or $D_{2d}$ symmetry descent. For known representations of ground states and JT active coordinates, it might be possible to determine the HPJT excited-state representations according to Equation (4). For the two-step symmetry descent, there are too many possibilities where almost all excited-state representations (except two-dimensional) might be involved. Therefore, we shall not deal with this problem.

## 4. Methods

We have performed geometry optimization of the complexes $^{m}$[dmaphPcAg]$^{q}$ with charges q = +1 → −2 in the two lowest spin states (singlet to quartet) with spin multiplicities m within the $D_{4h}$ symmetry and its subgroups. In agreement with our previous study [1], B3LYP hybrid functional [12], GD3 dispersion correction [13], cc-pVDZ-PP pseudopotential and basis set for Ag [14], and cc-pVDZ basis sets for remaining atoms [15] were used. The optimized structures were tested on the number of imaginary vibrations. Excited states (up to 50) were calculated for every optimized structure using time-dependent DFT (TD-DFT) treatment [16,17], analogously to our previous studies [1,18,19]. All calculations were performed with Gaussian16 (Revision B.01) software [20]. MOLDRAW (Release 2.0, https://www.moldraw.software.informer.com, accessed on 9 September 2019) software [21] was used for visualization and geometry modification purposes. Finally, a group-theoretical analysis of the obtained results was carried out using the methods of the epikernel principle [5–7] and of step-by-step symmetry descent [8,9].

The B3LYP functional is most frequently used in quantum-chemical studies and produces relatively reliable excitation energies. The basis sets used are restricted by our technical capabilities.

## 5. Conclusions

To shed more light on the photopolymerization action of the Ag(II) complex with dimethylamino phenyl-substituted phthalocyanine $^{2}$[dmaphPcAg]$^{0}$, we have performed a quantum-chemical model study of possible reaction intermediates [dmaphPcAg]$^{q}$ with charges q = +1 → −2, with the aim to explain the possible role of the JT effect. Group-theoretical analysis of the obtained results shows that the complexes under study are of two categories.

The stable structures of maximal symmetry of $^{1}$[dmaphPcAg]$^{+}$, $^{3}$[dmaphPcAg]$^{+}$, $^{2}$[dmaphPcAg]$^{0}$, and $^{4}$[dmaphPcAg]$^{2-}$ complexes (category I) correspond to the $D_4$ group as a consequence of the PJT effect within the unstable $D_{4h}$ structure. On the other hand, complexes $^{4}$[dmaphPcAg]$^{0}$, $^{1}$[dmaphPcAg]$^{-}$, $^{3}$[dmaphPcAg]$^{-}$, and $^{2}$[dmaphPcAg]$^{2-}$ (category II) with double degenerate electron ground states in (JT unstable) $D_{4h}$ symmetry structures undergo a symmetry descent to stable structures corresponding to maximal $D_2$ symmetry, not because of a simple JT effect but due to HPJT effect. The most stable reaction intermediate in the supposed photoinitiation reaction [1] is surprisingly $^{3}$[dmaphPcAg]$^{-}$ (a singlet electron state was expected). Therefore, the reduction of the $^{2}$[dmaphPcAg]$^{0}$ photoinitiator ($D_4$ symmetry) to the $^{3}$[dmaphPcAg]$^{-}$ intermediate ($D_2$ symmetry) must be significantly affected by vibronic interactions (PJT and HPJT effects), primarily the reaction barrier height and reaction equilibrium. Moreover, the reactivity of $^{3}$[dmaphPcAg]$^{-}$ is supported by the non-equal spin density at nitrogen atoms of the $D_2$ structure (doubled at one pair of these atoms; see Table S2 in Supplementary Materials). Nevertheless, their exact influence on reaction rates and thermodynamics must be investigated in solutions.

The presented study shows how group-theoretical treatment can be profitable through solving chemical problems for large molecules. The method of epikernel principle [5–7] is restricted to JT active coordinates based on perturbation theory and thus grants incomplete results, but it can also be used for the PJT effect. The method of step-by-step symmetry descent [8,9] based on splitting degenerate electron states during symmetry descent is more universal but not suitable for the PJT effect. We have shown the usefulness of the combination of both methods. Further theoretical studies in this field are welcome.

**Supplementary Materials:** The following supporting information can be downloaded at: https://www.mdpi.com/article/10.3390/molecules28207019/s1, Table S1. Relations between the irreducible representations of the parent group $D_{4h}$ and of its $D_4$ and $D_2$ subgroups. Table S2. Charge q, spin multiplicity m, symmetry group G, Mulliken atomic charges and spin populations of Ag and pyrrole N atoms in $^{m}$[dmaphPc]$^{q}$ complexes under study. Tables S3–S14. Atom coordinates of $^{m}$[dmaphPc]$^{q}$ in $D_{4h}$, $D_4$ or $D_2$ symmetry (in Å).

**Funding:** The work has been supported by the Slovak Research and Development Agency (no. APVV-19-0087), by the Slovak Scientific Grant Agency VEGA (no. 1/0139/20), and by Ministry of Education, Science, Research and Sport of the Slovak Republic within the scheme "Excellent research teams".

**Institutional Review Board Statement:** Not applicable.

**Informed Consent Statement:** Not applicable.

**Data Availability Statement:** Data are contained within the article.

**Acknowledgments:** The authors thank the HPC center at the Slovak University of Technology in Bratislava, which is a part of the Slovak Infrastructure of High Performance Computing (SIVVP project ITMS 26230120002, funded by European Region Development Funds) for the computational time and resources made available.

**Conflicts of Interest:** The funders had no role in the design of the study; in the collection, analyses, or interpretation of data; in the writing of the manuscript; or in the decision to publish the results.

**Sample Availability:** Not applicable.

## References


1. Breloy, L.; Alcay, Y.; Yilmaz, I.; Breza, M.; Bourgon, J.; Brezová, V.; Yagci, Y.; Versace, D.-L. Dimethyl amino phenyl substituted silver phthalocyanine as a UV- and visible-light absorbing photoinitiator: In situ preparation of silver/polymer nanocomposites. *Polym. Chem.* **2021**, *12*, 1273–1285. [CrossRef]
2. Jahn, H.A.; Teller, E. Stability of polyatomic molecules in degenerate electronic states. I. Orbital degeneracy. *Proc. R. Soc. London A* **1937**, *161*, 220–235.
3. Bersuker, I.B. Pseudo-Jahn–Teller Effect—A Two-State Paradigm in Formation, Deformation, and Transformation of Molecular Systems and Solids. *Chem. Rev.* **2013**, *113*, 1351–1390. [CrossRef] [PubMed]
4. Bersuker, I.B. Recent Developments in the Jahn–Teller Effect Theory. In *The Jahn-Teller Effect. Fundamentals and Implications for Physics and Chemistry*; Köppel, H., Yarkony, D.R., Barentzen, H., Eds.; Springer: Berlin/Heidelberg, Germany, 2009; pp. 3–24, ISBN 978-3642034312.
5. Ceulemans, A.; Beyens, D.; Vanquickenborne, L.G. Symmetry aspects of Jahn-Teller activity: Structure and reactivity. *J. Am. Chem. Soc.* **1984**, *106*, 5824–5837. [CrossRef]
6. Ceulemans, A.; Vanquickenborne, L.G. The Epikernel Principle. *Struct. Bonding* **1989**, *71*, 125–159.
7. Breza, M. Group-Theoretical Treatment of Pseudo-Jahn-Teller Systems. In *Vibronic Interactions and the Jahn-Teller Effect: Theory and Application*; Atanasov, M., Daul, C., Tregenna-Piggott, P.L.W., Eds.; Springer: Dordrecht, The Netherlands; Berlin/Heidelberg, Germany; London, UK; New York, NY, USA, 2012; pp. 59–82, ISBN 1567-7354.
8. Pelikán, P.; Breza, M. Classification of the possible symmetries of the Jahn—Teller systems. *Chem. Papers* **1984**, *39*, 255–270.
9. Breza, M. Group-Theoretical Analysis of Jahn-Teller Systems. In *The Jahn-Teller Effect. Fundamentals and Implications for Physics and Chemistry*; Köppel, H., Yarkony, D.R., Barentzen, H., Eds.; Springer: Berlin/Heidelberg, Germany, 2009; pp. 51–76, ISBN 978-3642034312.
10. Kaplan, I.G. Problems in DFT with the total spin and degenerate states. *Int. J. Quantum Chem.* **2007**, *107*, 2595–2603. [CrossRef]
11. Schurkus, H.F.; Chan, G.K.-L.; Chen, G.-T.; Cheng, H.-P.; Stanton, J.F. Theoretical prediction of magnetic exchange coupling constants from broken-symmetry coupled cluster calculations. *J. Chem. Phys.* **2020**, *152*, 234115. [CrossRef] [PubMed]
12. Becke, A.D. Density-functional thermochemistry. III. The role of exact exchange. *J. Chem. Phys.* **1993**, *98*, 5648–5652. [CrossRef]
13. Grimme, S.; Antony, J.; Ehrlich, S.; Krieg, H. A consistent and accurate ab initio parameterization of density functional dispersion correction (DFT-D) for the 94 elements H-Pu. *J. Chem. Phys.* **2010**, *132*, 154104. [CrossRef] [PubMed]
14. Pritchard, B.P.; Altarawy, D.; Didier, B.; Gibson, T.D.; Windus, T.L. New Basis Set Exchange: An Open, Up-to-Date Resource for the Molecular Sciences Community. *J. Chem. Inf. Model.* **2019**, *59*, 4814–4820. [CrossRef] [PubMed]
15. Dunning, T.H., Jr. Gaussian basis sets for use in correlated molecular calculations. I. The atoms boron through neon and hydrogen. *J. Chem. Phys.* **1989**, *90*, 1007–1023. [CrossRef]
16. Bauernschmitt, R.; Ahlrichs, R. Treatment of electronic excitations within the adiabatic approximation of time dependent density functional theory. *Chem. Phys. Lett.* **1996**, *256*, 454–464. [CrossRef]
17. Scalmani, G.; Frisch, M.J.; Mennucci, B.; Tomasi, J.; Cammi, R.; Barone, V. Geometries and properties of excited states in the gas phase and in solution: Theory and application of a time-dependent density functional theory polarizable continuum model. *J. Chem. Phys.* **2006**, *124*, 94107. [CrossRef] [PubMed]
18. Štellerová, D.; Lukeš, V.; Breza, M. How does pseudo-Jahn-Teller effect induce the photoprotective potential of curcumin? *Molecules* **2023**, *28*, 2946. [CrossRef] [PubMed]
19. Štellerová, D.; Lukeš, V.; Breza, M. On the Potential Role of (Pseudo-) Jahn-Teller Effect in Membrane Transport Processes: Enniatin B and Beauvericin. *Molecules* **2023**, *28*, 6264. [CrossRef] [PubMed]
20. Frisch, G.W.; Trucks, M.J.; Schlegel, H.B.; Scuseria, G.E.; Robb, M.A.; Cheeseman, J.R.; Scalmani, G.; Barone, V.; Petersson, G.A.; Nakatsuji, H.; et al. *Gaussian 16, Revision B.01*; Gaussian, Inc.: Wallingford, CT, USA, 2016.
21. Ugliengo, P. MOLDRAW: A Program to Display and Manipulate Molecular and Crystal Structures (Release 2.0), University Torino, Torino. 2012. Available online: https://www.moldraw.software.informer.com (accessed on 9 September 2019).